

Mechanics of Patterned Helical Si Springs on Si Substrate

D.-L. Liu,^a D.-X. Ye,^a F. Khan,^b F. Tang,^a B.-K. Lim,^c R. C. Picu,^b G.-C. Wang,^a and T.-M. Lu^{a,*}

^aDepartment of Physics, Applied Physics, and Astronomy, Rensselaer Polytechnic Institute, Troy, New York, USA

^bDepartment of Mechanical, Aerospace and Nuclear Engineering, Rensselaer Polytechnic Institute, Troy, New York, USA

^cDepartment of Materials Engineering, Nanyang Technological University, Singapore

The elastic response, including the spring constant, of individual Si helical-shape submicron springs, was measured using a tip-cantilever assembly attached to a conventional atomic force microscope. The isolated, four-turn Si springs were fabricated using oblique angle deposition with substrate rotation, also known as the glancing angle deposition, on a templated Si substrate. The response of the structures was modeled using finite elements, and it was shown that the conventional formulae for the spring constant required modifications before they could be used for the loading scheme used in the present experiment.

Keywords: Si, Templated Si, Spring, Oblique Angle Deposition, Glancing Angle Deposition, Spring Constant, Atomic Force Microscope, Finite Element, Loading.

The emerging field of nanotechnology requires basic understanding of the physical, electrical, and optical properties of smaller and smaller volumes of materials. In particular, knowledge of the mechanical behavior of materials in the submicron scale range is essential for building useful micro- and nanomachines. However, both the fabrication of suitable submicron size test structures and the measurement of their mechanical properties are challenging. In the present work, we show that it is possible to measure the elastic behavior, including the spring constant, of individual Si helical-shape submicron springs, using a tip-cantilever assembly attached to a conventional atomic force microscope (AFM). The isolated, four-turn Si springs were fabricated using oblique angle deposition with substrate rotation,^{1,2} also known as the glancing angle deposition, on a templated Si substrate.

To date, most mechanical measurements of individual (isolated) submicron scale structures have focused on carbon nanotubes,^{3,4} coiled nanotubes,⁴ nanowires,⁵ and nanocrystals.⁶ A suitable technique was needed to measure the mechanical properties of another very basic mechanical element, the helical-shaped spring. Attempts had been made to measure the elastic properties of densely packed helical nanostructures with the nanoindentation technique.^{7,8} However, the tip in a conventional nanoindentation device is rather large and cannot be used effectively as an imaging tool to locate the individual position of the springs. Also, when a sample contains closely connected nanostructures, the nature of the load on a single nanostructure is not well

defined, and one can only estimate an average value of the spring constant.

Figures 1a (spring A) and 1b (spring B) show the scanning electron microscopy (SEM) cross section images of the well-separated Si helical spring samples we grew and used in this work. The samples were prepared on a templated Si substrate by the oblique angle deposition technique with substrate rotation at room temperature. The template consisted of a two-dimensional array of W posts in square and triangular patterns on which spring A (Fig. 1a) and spring B (Fig. 1b) were grown, respectively. The cylindrical W posts have an average diameter of 150 nm, and the post-to-post distances are 1,000 nm and 600 nm for the square (Fig. 1a) and triangular patterns (Fig. 1b), respectively. In Figure 1b, not all the springs are in the same plane (depth) because of the triangular symmetry of the template (every other spring is behind). Figure 2a is a SEM top view of the springs shown in Figure 1a grown on the square patterned template. Figure 2b is a noncontact AFM top view of the springs shown in Figure 1a. The deposition was performed in a high vacuum chamber with a base pressure of 4×10^{-5} Pa. The incident angle of the Si vapor flux with respect to the substrate surface normal was fixed at 85°. The substrate rotational speed was 2 h/turn, and each turn was divided into 32 discrete steps. The growth rate was about 0.55 nm/s. The rising angle (or pitch angle) of the springs is 28°. The pitch is $h = 950$ nm. The wire thicknesses (diameter, t) of the springs were measured to be 350 ± 20 and 225 ± 10 nm for spring A and spring B, respectively. The mean coil diameters (D) are 570 ± 30 and 590 ± 10 nm for spring A and spring B, respectively.

*Author to whom correspondence should be addressed.

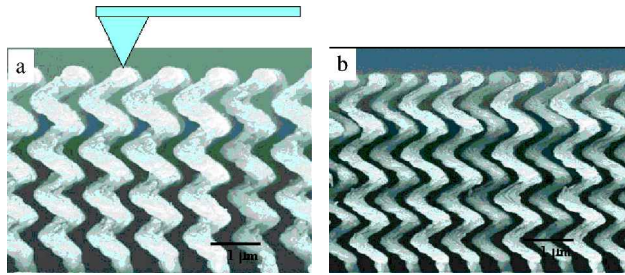


Fig. 1. (a) (spring A) and (b) (spring B) show scanning electron micrographs (cross-sections) of the Si helical submicron springs (about 4 μm high) on square and triangular patterned Si substrates prepared by oblique angle deposition with substrate rotation. In Figure 1a we also show a schematic diagram of the loading of the AFM tip.

The Si springs are amorphous in nature because the deposition was carried out at room temperature. The AFM silicon cantilever with a monocrystalline silicon conical tip used in this experiment has a spring constant of 17 N/m. The tip height is nominally 5–7 μm, and the tip radius of curvature is about 10 nm.

First we used noncontact mode AFM to image the sample surface. This allowed us to precisely target the application of the compressive load onto a single spring structure and apply the load with the same tip. (See the schematic diagram of the tip in Fig. 1a.) In Figure 2b, the circular spot indicates the position on the spring where the load is applied. The compression was achieved by controlling the vertical movement (z) of the substrate against the AFM tip. The amount of compression or displacement, d , of the spring was equal to the difference between z and the deflection of the cantilever. The force applied was evaluated as the product of the cantilever spring constant and its deflection. The force versus spring displacement curves for 20 individual springs for each pattern shown in Figure 1a and b were measured. Representative curves of loading (filled triangles) and unloading (open squares) for each type of spring are shown in Figure 3. The loading speed was 100 nm/s. The loading and unloading curves are seen to be linear and reversible, indicating linear elastic behavior within this range of displacement. Hence, no rate effects are expected. The average

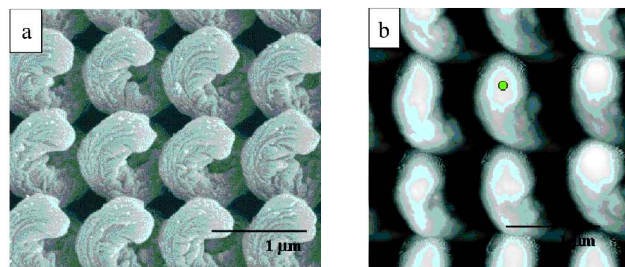


Fig. 2. (a) A top view SEM image of the spring A shown in Figure 1a grown on the square patterned template. (b) A top view noncontact AFM image of spring A shown in Figure 1a. The solid dot shows the position where the load is applied.

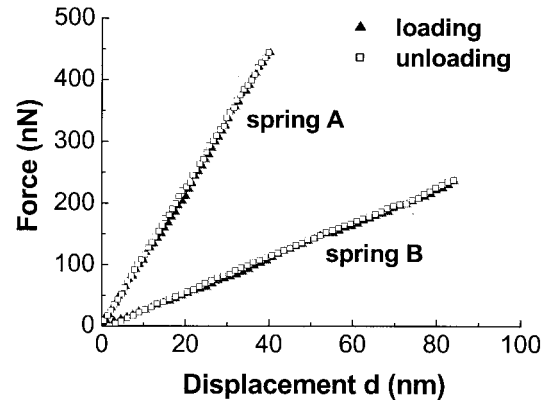


Fig. 3. Representative loading (filled triangles) and unloading (open squares) force versus displacement curves for spring A and spring B.

spring constant of the type shown in Figure 1a was measured to be 10.2 N/m with a standard deviation of 1.5 N/m, whereas for the type shown in Figure 1b it was 2.8 N/m with a standard deviation of 0.6 N/m. In Figure 4a and b we plot the statistical histograms of the measured spring constant for the springs shown in Figure 1a and b, respectively. The peak positions of the histograms are at about 10.5 N/m for spring A and 3.1 N/m for spring B, which are close to the average spring constant values for each type.

No indentation occurred, and the value d obtained from the experiment was totally due to the spring displacement.

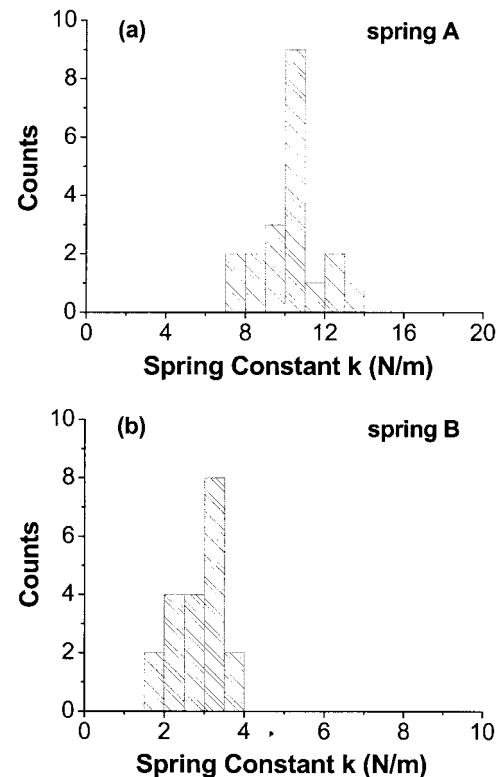


Fig. 4. Statistical histograms of the measured spring constants are shown in (a) for spring A and (b) for spring B.

This was confirmed by a separate experiment in which we used the same tip to indent into a blanket amorphous Si thin film sample of 1,400 nm thick with the maximum force used in this work. The vertical displacement of the substrate, z , was identical to the deflection of the cantilever with no film indentation.

The ability of the conventional formula for the spring constant commonly used in the design of mechanical components to quantitatively describe our experimental results was tested. The formula that predicts the constant in terms of the ratio of the wire to coil diameter, t/D , for large pitch angles, reads⁹

$$k = \frac{Gt^4}{8D^3n} \left[1 - \frac{3t^2}{16D^2} + \frac{3+\nu}{2(1+\nu)} \tan^2(\alpha) \right]^{-1} \quad (1)$$

where n is the number of turns of the spring, and G is the shear modulus. The shear modulus and the Young's modulus, E , are related by $G = E/2(1 + \nu)$, where ν is the Poisson's ratio. The angle α may be evaluated based on the wire and coil diameters and the pitch of the spring, h , as

$$\tan \alpha = \frac{h}{\pi(D+t)} \quad (2)$$

The Young's modulus, E , was measured in a separate indentation experiment using an amorphous Si continuous film (no annealing) grown under similar conditions without substrate rotation. A stiff cantilever of 445 N/m was used for this measurement for an indentation depth up to 20 nm. The modulus was inferred from the measured force versus penetration curve using the Hertzian contact model, and a value of $E = 45$ GPa was obtained. The Poisson's ratio was taken to be $\nu = 0.22$ (from Ref. 10). For comparison, the same tip was used to indent a Si(100) wafer and we obtained a value of $E = 120$ GPa, which is very close to the modulus of a single crystal Si(100) (130 GPa) reported in the literature.¹¹

The spring constant of the two types of springs was evaluated with Eqs. (1) and (2) for the range of geometrical parameters measured from Figure 1. The computed values overestimate the measured spring constant by more than 100%. To elucidate the origins of this discrepancy, the springs were modeled by finite elements (FEM). Models were developed for two springs from each type. One spring had the smallest t and largest D of the range (e.g., $t = 330$ nm and $D = 600$ nm for type A), whereas the other had the largest t and smallest D for that particular spring type (e.g., $t = 370$ nm and $D = 540$ nm for type A). Therefore, the spring constants of the two modeled springs bracket the range of spring constants to be expected for the respective spring type. The results are shown in Figure 5 as pairs of lines labeled A and B, respectively. The force was first applied along the axis of the coil (labeled "Axial force" in Fig. 5). It was observed that in this case the prediction of the spring constant by Equation (1) is very close to that obtained by the FEM analysis. Therefore, both the

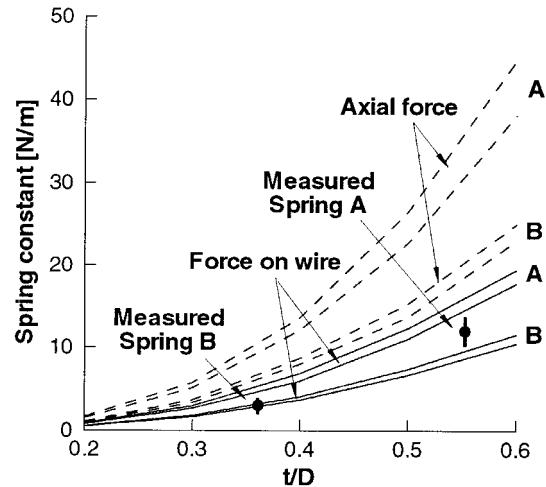


Fig. 5. Variation of the spring constant with the ratio of the wire to coil diameters, t/D . The pairs of lines labeled A and B bracket the range of function values corresponding to the range of uncertainty of the geometrical parameters of each spring type. Two sets of such curves are presented. Those labeled "Axial force" (dashed curves) correspond to the loading of the springs by a force acting along the axis of the coil, whereas "Force on wire" (solid curves) designates the situation in which the force acts directly on the wire of the spring (off-axis). The measured values of the effective spring constants for type A and B springs are shown as data points (filled circles with error bars).

FEM model and Eq. (1) severely overestimate the experimental results (shown as data points in Fig. 5).

When the force is applied directly on the wire of the spring, as in the actual experiments, the structure is subjected to axial compression as well as to bending. The displacement of the point where the force acts is rather large in all directions; however, the effective spring constant may be evaluated by dividing the force (oriented in the direction of the axis of the coil) by¹ the displacement component in the force direction. This loading mode was modeled by finite elements, and the results are shown in Figure 5 (labeled "Force on wire"). The effective spring constant is seen to be much smaller than that evaluated for axial loading and in reasonable agreement with the experimental results. Therefore, it is concluded that linear elasticity may be used to predict the response of these structures provided that the geometrical parameters and loading conditions are properly represented in the model.

Acknowledgments: This work was supported in part by the National Science Foundation. We thank Professor Paul Ho and Professor Theodorian Borca-Tasciuc for valuable discussions on the application of the nanoindentation technique.

References and Notes

1. Y.-P. Zhao, D.-X. Ye, P.-I. Wang, G.-C. Wang, and T.-M. Lu, *Int. J. Nanosci.* 1, 87 (2002).

2. S. R. Kennedy, M. J. Brett, O. Toader, and S. John, *NanoLett.* **2**, 59 (2002).
3. J.-P. Salvetat, J.-M. Bonard, A. J. Kulik, L. Forró, and L. Zuppiroli, *Appl. Phys. A* **69**, 255 (1999).
4. A. Volodin, M. Ahlskog, E. Seynaeve, and C. V. Haesendonck, *Phys. Rev. Lett.* **84**, 3342 (2000).
5. E. W. Wong, P. E. Sheehan, and C. M. Liebert, *Science* **277**, 1971 (1997).
6. C. Durkan, A. Ilie, M. S. M. Saifullah, and M. E. Welland, *Appl. Phys. Lett.* **80**, 4244 (2002).
7. M. W. Seto, D. Dick, and M. J. Brett, *J. Micromech. Microeng.* **11**, 582 (2001).
8. M. W. Seto, K. Robbie, D. Vick, and M. J. Brett, *J. Vac. Sci. Technol. B* **17**, 2172 (1999).
9. C. J. Ancker and J. N. Goodier, *J. Appl. Mech.* **25**, 466 (1958).
10. T. Searle (ed.), *Properties of Amorphous Si and its Alloys*, Inspec, London, p. 359 (1998), p. 359.
11. G. Simmons and H. Wang, *Single Crystal Elastic Constants and Calculated Aggregate Properties*, MIT Press, Cambridge, MA, (1971), p. 85.

Received: 24 May 2003. Revised/Accepted: 16 June 2003.